Control Engineering Practice 132 (2023) 105420

Contents lists available at ScienceDirect

Control Engineering Practice

journal homepage: www.elsevier.com/locate/conengprac

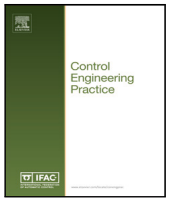

Systematic modeling of complex time-variant gear systems using a Power-Oriented approach

Davide Tebaldi *, Roberto Zanasi

University of Modena and Reggio Emilia, Department of Engineering "Enzo Ferrari", Via Pietro Vivarelli 10 - int. 1, 41125 Modena, Italy

ARTICLE INFO

Keywords:
Automotive systems
Gear systems
Time-variant systems
Energetic modeling
Power-Oriented Graphs
Simulation

ABSTRACT

This paper addresses a methodology for the systematic modeling of complex gear systems. The methodology is based on the use of a unified general model, working for all complex gear systems: time-variant as well as time-invariant, having parallel or oblique rotation axes. The model equations are automatically written following the outlined procedure and applying the presented algorithms, making this approach less prone to mistakes with respect to other approaches. Next, a reduced model assuming rigid gear connections and introducing no loss of information is proposed, which directly gives the kinematic relations between the gears angular speeds and input torques. In order to show some case studies, the proposed methodology is applied to three systems of interest for vehicle dynamics and powertrain modeling. The considered case studies are a differential structure having a bevel gearing system with non-perpendicular gear shafts, a vehicle differential and a full toroidal variator, which is suitable for applications such as KERS (Kinetic Energy Recovery System) and IVT (Infinitely Variable Transmission). Furthermore, the control of a full toroidal variator acting as a KERS with reference to an automotive case study and the comparison of the proposed modeling methodology with two other approaches are addressed.

1. Introduction

Transportation systems are an important part of nowadays human life, with particular reference to road transportation systems, significantly impacting our daily life. In the last two decades, the growing awareness of climate changes has led to the investment of great resources for research in the field of Hybrid Electric Vehicles (HEVs) (He, Shou, & Wang, 2022; Miller, 2006; Zhang, Liu, et al., 2020). The articulated process leading to the design and development of a new vehicle passes through a large number of steps and can differentiate depending on the type of vehicle. A first important step consists in the identification of the most suitable vehicle architecture. In the field of HEVs, a large variety of architectures and topologies are available in the literature, including series HEVs (Chen, Evangelou, & Lot, 2019), parallel HEVs (Kim & Choi, 2020), power-split HEVs (Gong et al., 2021; Tebaldi & Zanasi, 2019, 2021) and plug-in HEVs (Oncken, Sachdeva, Wang, & Chen, 2021).

Once the most suitable architecture has been identified, the modeling step has to be addressed. Modeling a vehicle architecture is an essential part, as it enables the simulation, testing and performance evaluation of the vehicle before its physical production. A vehicle can be seen as a complex physical system, composed of several physical subsystems (Khajepour, Fallah, & Goodarzi, 2014) interacting with each other. As far as the modeling of the powertrain is concerned, an important part is covered by gear systems, which are included in many physical elements of the powertrain. A first example of physical elements in the powertrain including gear systems are differentials (Khajepour et al., 2014), which are responsible for distributing the motive torque among the left and the right axles. A second example are planetary gear sets (Hou & Ji, 2021; Khajepour et al., 2014; Mishra & Srinivasan, 2017; Ouyang et al., 2022), which represent a key component of automatic transmissions and ECVTs (Electro Continuously Variable Transmissions). A third example are toroidal variators (Khajepour et al., 2014; Patil, 2011), which can be half or full and can be exploited to implement a KERS (Kinetic Energy Recovery System) as well as an IVT (Infinitely Variable Transmission). There are also many other elements in the powertrain transmission system, which can include more complicated gear systems, such as transmissions including bevel gearing systems for example (Du, Mao, Cui, Liu, & Zhao, 2018), which are employed to transmit power between non-parallel shafts. Furthermore, gearing systems are highly employed in other transportation fields (Molyneux, 1997) as well as in other engineering fields, such as mechatronic machines and robotics.

There are several different approaches in the literature for modeling these devices. The modeling of differentials is addressed in Forstinger, Bauer, Hofer, and Rossegger (2016) making some simplifying assumptions to develop a reduced model. A simple modeling is performed

* Corresponding author.
E-mail addresses: davide.tebaldi@unimore.it (D. Tebaldi), roberto.zanasi@unimore.it (R. Zanasi).

https://doi.org/10.1016/j.conengprac.2022.105420
Received 4 May 2022; Received in revised form 11 September 2022; Accepted 15 December 2022
Available online xxxx
0967-0661/

in Gadola and Chindamo (2018), where the working principles, advantages and limitations of passive limited-slip differentials are discussed. One of the most widespread platforms for modeling powertrains is provided by the Mathworks tools. The "Open Differential" (S., 0000a) and the "Limited Slip Differential" (S., 0000b) blocks, that are found in the Powertrain Blockset and in the Vehicle Dynamics Blockset provided by Simulink, model the differential employing the differential equations describing it under the assumption of rigid coupling between the crown gear and the axles and neglecting the dynamics of the differential box and of the planetaries. Let us now consider planetary gear sets, for which different modeling approaches can be found in the literature. As an example, an approach for determining the kinematics of a coupled epicyclic spur-gear train is proposed in Freudenstein and Yang (1972). Later on, the Lever Analogy (Benford & Leising, 1981) was introduced, which is still one of the most employed tools for the kinematic and dynamic analysis of planetary gear sets. Other approaches can be found, adopting different degrees of simplification, including the use of basic physics laws assuming rigid connections employed in Zhang, Shen, and Kako (2020) for the modeling of the planetary gear set, for instance. As far as toroidal variators are concerned, an interesting approach for modeling a full toroidal variator is presented in Fuchs, Hasuda, and James (2002), which consists in a velocity analysis at the contact points, followed by the modeling of the traction forces and by the Newtonian formulation of the equation of motion on the roller. In Newall, Cowperthwaite, Hough, and Lee (2005), the authors chose to focus on the efficiency modeling instead, by combining a full EHL (ElastoHydrodynamic Lubricated) model, an empirical traction model and a variator cooling model. Physical elements in different energetic domains can also be modeled with an energetic approach using different modeling techniques, including Bond Graphs (Cauffriez, Grondel, Loslever, & Aubrun, 2016; Jha, Dauphin-Tanguy, & Ould-Bouamama, 2018), Energetic Macroscopic Representation (García-Herreros, Kestelyn, Gomand, Coleman, & Barre, 2013; Lhomme et al., 2017), and Power-Oriented Graphs (Zanasi, 2010; Zanasi, Grossi, & Fei, 2014). A comparison of the main properties of these techniques can be found in Zanasi, Geitner, Bouscayrol, and Lhomme (2008). In this paper, the Power-Oriented Graphs (POG) technique is used, since it is deemed to be very effective when developing the systematic procedure illustrated in this paper. Some applications of this technique are in Tebaldi and Zanasi (2019), Zanasi et al. (2014), (Zanasi & Tebaldi, 2019, 2020a, 2020b).

In this paper, we would like to extend the systematic methodology for modeling planetary gear sets at a system level introduced in our previous work (Zanasi & Tebaldi, 2019, 2020a, 2020b). Such methodology has the following main features (Zanasi & Tebaldi, 2020a) with respect to the state of the art: (a) the proposed dynamic model is general, i.e. it can be used for modeling any planetary gear set and can be directly implemented in the Matlab/Simulink environment; (b) the procedure for building the system matrices and vectors is *fully systematic*, thus reducing the chances of making mistakes when deriving the system model; (c) relative frictions can be freely inserted between any couple of gears, thus enabling the simulation of different transmission operating modes; (d) two dynamic models are automatically given: a full elastic model and a reduced rigid model; (e) the reduced rigid model is very suitable for real-time simulations and introduces no loss of information since the tangential forces can still be recovered, even when the gears are assumed to be rigidly coupled. Furthermore, the kinematic constraints and torque relations automatically result from the reduced model. The contributions of this paper with respect to the previous work are illustrated in detail in Section 2.

With respect to other approaches in the literature, such as the Lagrangian approach for example, our approach offers the following benefits. First, the system equations are automatically written, which makes the approach less prone to mistakes. Second, the approach is always the same for any type of system, both time-invariant and time-variant, and is therefore unified and more general. Third, two system models are automatically obtained: a full one, giving a more detailed description of the system including the gears elastic interaction, and a reduced one assuming rigid connections. The reduced order model automatically gives the kinematic relations between the gears angular speeds and input torques and is more suitable for fixed-step size simulations for real-time executions, as it does not contain the stiffnesses fast dynamics. Furthermore, the time behavior of the forces exchanged between the gears can still be computed using the reduced model. The approach proposed in this paper also offers advantages with respect to other dedicated models made available by some well-known simulation platforms, e.g. the Matlab/Simulink open differential model.

The remainder of this paper is structured as follows. The contributions with respect to the previous work are detailed in Section 2, whereas the symbol notations and the nomenclature employed throughout the paper are summarized in Section 3. Section 4 contains the formal definition of the systematic methodology for modeling complex time-variant gear trains, together with the extended algorithm for the automatic computation for the radii matrix $\mathbf{R}(t)$, the reduced model definition and the formula for recovering the gears contact forces in the reduced model. Three case studies are addressed in the next sections: a fictitious oblique differential structure in Section 5-(1), a vehicle differential in Section 5-(2) and Section 5-(3) and the modeling, control and simulation of a full toroidal variator in Section 6. The contributions of our approach with respect to two other solutions in the literature are illustrated in detail in Section 7. Finally, the conclusions of this study are reported in Section 8, the algorithm for the systematic computation of the relative friction matrix $\mathbf{B}_{\Delta\omega}$ is given in Appendix A and the proof of Property 2 is given in Appendix B.

2. Contributions with respect to the previous work

With respect to our previous work, we provide the following new contributions in this paper: (a) the formal definition of the systematic modeling process which is unified for any generic time-variant gear system composed of n_J gears, n_K elastic couplings between the gears and n_B relative frictions between the gears. This formal definition is made by abstracting from the specific case studies in order to make it more general, see Section 4; (b) a unified Matlab/Simulink structure suitable for simulating both the full and the reduced model of any linear time-variant or time-invariant gear system; (c) the extension and application of the systematic methodology not only to the modeling of planetary gear sets, as it was instead in the previous work, but also to the modeling of generic complex gear systems. These can therefore include planetary, parallel and oblique rotation axes (e.g. differentials, toroidal variators, etc.), see the new Algorithm 1 in Section 4.1; (d) the extension and application of the systematic methodology to the modeling of time-variant gear systems, which were not accounted for in the previous work, see the new Algorithm 1 in Section 4.1; (e) the proof that the tangential forces being present at the gears contact points can still be recovered in the reduced rigid system even in the time-variant case, see the new Property 2 which holds true for the time-variant case as well, on the contrary with respect to the previous work; (f) the modeling of three new case studies which were not present in the previous work. The three new case studies are: a differential with oblique rotation axes, a vehicle differential and a full toroidal variator. These case studies show the extension and application of the new systematic methodology to the modeling of more generic and complex gear systems, including parallel and oblique rotation axes and the time-variant case; (g) a new approach to control a full toroidal variator when employed as a KERS, namely as a Kinetic Energy Recovery System, together with an automotive example showing the KERS and its control operations; (h) the contributions of our approach with respect to two other different approaches in the literature.

3. Notations and nomenclature

Notations

$\mathcal{N} = \{i\}$	Ordered set containing elements i;
$\mathcal{N} = \{ij\}$	Ordered set containing couples ij;
$\mathcal{N} = \{ij{=}\{ij\}\}$	Ordered set containing ordered couples $\{ij\}$;
$\underset{\mathcal{N}}{\overset{i}{\left\|\left[x_i\right]\right\|}} = \begin{bmatrix} x_a \\ x_b \\ x_c \\ \vdots \end{bmatrix}$, $\underset{\mathcal{N}}{\overset{i}{\left\|\left[x_i\right]\right\|}} = \begin{bmatrix} x_a & 0 & 0 & 0 \\ 0 & x_b & 0 & 0 \\ 0 & 0 & x_c & 0 \\ 0 & 0 & 0 & \ddots \end{bmatrix}$, with $\mathcal{N} = \{a, b, c, \ldots\}$;	
$\mathbf{I}$	Identity matrix of proper dimension;
$\ker(\mathbf{A})$	Kernel of matrix ($\mathbf{A}$);
$\mathrm{Im}(\mathbf{A})$	Image of matrix ($\mathbf{A}$);

Nomenclature

System Definition

$\mathcal{N}_J$	Ordered set containing the one-digit subscripts i identifying the n_J system gears;
$\mathcal{N}_K$	Ordered set containing the two-digit ordered subscripts $ij = \{ij\}$ identifying the n_K system tangential springs;
$\mathcal{N}_B$	Ordered set containing all the n_B two-digit subscripts ij identifying the system relative frictions;
J_i, b_i, ω_i, τ_i	Moment of inertia, linear friction coefficient, angular speed and input torque of gear "i";
K_{ij}, d_{ij}, F_{ij}	Stiffness coefficient, linear friction coefficient, force of tangential spring "ij";
b_{ij}	Relative friction coefficient between gears "i" and "j";
$\mathbf{L}$, $\mathbf{A}(t)$, $\mathbf{B}$	Energy, power and input matrices;
$\mathbf{J}$, $\mathbf{K}$	Inertia and stiffness matrices;
$\mathbf{B}_J$, $\mathbf{B}_\omega$, $\mathbf{B}_{\Delta\omega}$, $\mathbf{B}_K$	Inertia, gears, relative and stiffness friction matrices;
$\mathbf{R}(t)$	Radii matrix;
$\mathbf{x}$, $\boldsymbol{\omega}$, $\mathbf{F}$	State, speed and force vectors;
$\mathbf{u} = \boldsymbol{\tau}$, $\mathbf{y} = \boldsymbol{\omega}$	Input torque and output speed vectors;
E_s, P_d	Stored energy and dissipated power within the system;

Algorithm 1

$r_{ij,h}(t)$	Generic coefficient of matrix $\mathbf{R} = [r_{ij,h}(t)]$, with $ij \in \mathcal{N}_K$ and $h \in \mathcal{N}_J$;
$r_h(t)$	Effective radius linking the angular speed ω_h to the tangential force F_{ij};
$\theta(t)$	Parameter giving the dependence of $r_h(t)$ on time;
$S_{F_{ij}}$	Sign related to the positive orientation of vector F_{ij};
S_{ω_h}	Sign related to the positive orientation of vector ω_h;

Reduced Rigid Model

$\mathbf{x}_1$	State vector of the reduced rigid model;
$\mathbf{T}_1(t)$	Rectangular transformation matrix relating $\mathbf{x}$ to $\mathbf{x}_1$;
$\mathbf{Q}_1(t)$	Matrix expressing the n_J original angular speeds as a function of the $n_J - n_K$ angular speeds in $\mathbf{x}_1$;
$\mathbf{L}_1(t), \mathbf{N}_1(t), \mathbf{A}_1(t), \mathbf{B}_1(t)$	Matrices of the reduced rigid model;

Full Toroidal Variator Reduced Model

$R_{a\theta}$, R_b, $R_{c\theta}$, R_d	Ratios between angular speeds;
$J(t)$, $N(t)$, $A(t)$	Scalar time-variant parameters of the full toroidal variator reduced model;
ω_d	Angular speed in the reduced state vector;
τ_d	System input torque;

Kinetic Energy Recovery System (KERS) Control

K_d	Torsional spring connecting the KERS to the vehicle transmission shaft;
ω_t	Transmission shaft angular speed;
$\theta(t)$	Position of the KERS rollers;
τ_{des}	Desired profile for input torque τ_d;
K_θ, K_w	Parameters of the KERS integral control;
Δ_τ	Tracking error of input torque τ_d;
Δ_ω	Tracking error of angular speed ω_d;
$\tilde{\tau}_d$	Estimation of input torque τ_d;
$\dot{E}$	Time derivative of the energy stored in the KERS;

Extended Lagrangian Equations

N	Number of the system degrees of freedom;
q_i	Generalized Lagrangian coordinates;
Q_i	Generalized forces;
T, U	System kinetic and potential energies;
θ_d	Angular position of time-variant inertia $J(t)$;

Algorithm 2

B_{ij}	Generic coefficient of matrix $\mathbf{B}_{\Delta\omega} = [B_{ij}]$, with $i, j \in \mathcal{N}_J$;
$\mathcal{N}_i$	Set of all the subscripts $pq \in \mathcal{N}_B$ such that $p = i$ or $q = i$;
$\bar{b}_{ij}$, S_{ij}	Relative friction coefficient and sign function defined in Appendix A.

4. Modeling a time-variant gear system

This section is focused on the description of the proposed general mathematical model which can be used for different types of gear systems. Let us consider a system composed of a generic number n_J of gears. Each gear is uniquely identified by a one-digit subscript "i". The interaction between the gears takes place through a number n_K of elastic contact points, which are modeled as tangential springs. Each tangential spring is uniquely identified by a two-digit *ordered* subscript "$ij = \{ij\}$". The latter is said to be ordered because it describes the positive *direction* of the spring (Zanasi & Tebaldi, 2020a), whose first and second terminals are connected to gear i and to gear j, respectively. This can be clearly seen from the example reported in Fig. 1. The figure also highlights that the exchanged force F_{ab} is tangential to the gears themselves, which is why the gears contact points are said to be coupled by *tangential springs*. If two gears i and j are arranged in a mechanical configuration causing the presence of some relative friction between them, a two-digit subscript ij is assigned to the considered relative friction. According to what has been described so far, let us define the

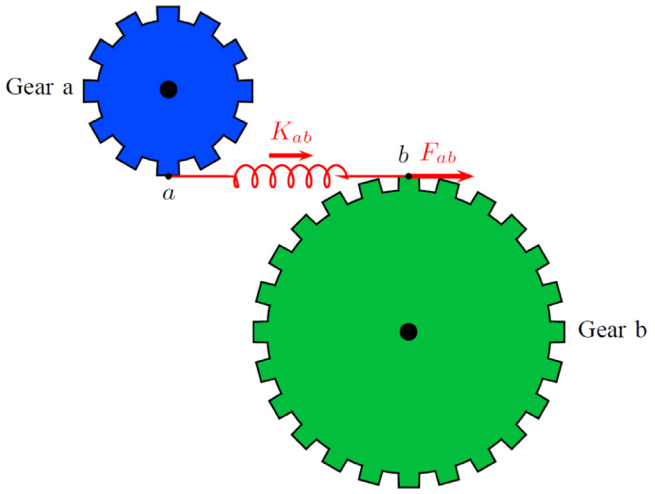

Fig. 1. Tangential spring K_{ab} coupling gears a and b.

following sets:

$$\begin{aligned}&\mathcal{N}_J=\{a,\ b,\ c,\ \dots\},\\&\mathcal{N}_K=\left\{ij=\{ij\},\ \forall i,j\in\mathcal{N}_J\,|\,(i\neq j)\wedge(\{ji\}\notin\mathcal{N}_K)\right\},\\&\mathcal{N}_B=\left\{ij,\ \forall i,j\in\mathcal{N}_J|(i\neq j)\wedge(ji\notin\mathcal{N}_B)\right\}.\end{aligned}\tag{1}$$

$\mathcal{N}_J$ is the ordered set containing the one-digit subscripts i identifying the n_J gears in the system, whereas $\mathcal{N}_K$ is the ordered set containing the two-digit ordered subscripts $ij=\{ij\}$ identifying the n_K tangential springs in the system. Hereinafter, the shorter notation ij will be adopted for the two-digit ordered subscripts belonging to set $\mathcal{N}_K$ for the sake of brevity. Lastly, $\mathcal{N}_B$ is the ordered set containing all the n_B two-digit subscripts ij identifying the relative frictions present in the system. The sets $\mathcal{N}_J$, $\mathcal{N}_K$ and $\mathcal{N}_B$ are said to be ordered because the order of the subscripts they contain will define the order of the parameters within the system matrices and vectors, as described in the remainder of this section. This does not impact the system dynamics in any way, but simply changes the order in which the system energetic ports appear in the system model. With reference to the simple two-gears system reported in Fig. 1 as an example, it is $\mathcal{N}_J=\{a,b\}$, $\mathcal{N}_K=\{ab\}$, $\mathcal{N}_B=\{\}$. The one-digit subscripts $i\in\mathcal{N}_J$ characterize all the parameters and variables associated with the gears: J_i and b_i are the moment of inertia and the linear friction coefficient of gear i, ω_i and τ_i are its angular speed and input torque. The positive direction of the angular speeds ω_i and of the input torques τ_i is chosen to be the same. This ensures a positive power flow entering the system through gear i when both ω_i and τ_i are positive, and viceversa. The two-digit ordered subscripts $ij\in\mathcal{N}_K$ denote all the parameters and variables associated with the tangential springs: K_{ij} and d_{ij} are the stiffness coefficient and the linear friction coefficient of spring ij, while F_{ij} is its tangential force. The force F_{ij} will be positive when transmitted from gear i to gear j through the spring, and viceversa.

Any gear system having time-variant interactions between the gears can be modeled using the following general POG state–space model:

$$\underbrace{\begin{bmatrix}\mathbf{J}&\mathbf{0}\\\mathbf{0}&\mathbf{K}^{-1}\end{bmatrix}}_{\mathbf{L}}\dot{\mathbf{x}}=\underbrace{\begin{bmatrix}-\mathbf{B}_J-\mathbf{R}^{\mathrm{T}}(t)\mathbf{B}_K\mathbf{R}(t)&-\mathbf{R}^{\mathrm{T}}(t)\\\mathbf{R}(t)&\mathbf{0}\end{bmatrix}}_{\mathbf{A}(t)}\mathbf{x}+\underbrace{\begin{bmatrix}\mathbf{I}\\\mathbf{0}\end{bmatrix}}_{\mathbf{B}}\underbrace{\mathbf{u}}_{\boldsymbol{\tau}},\tag{2}$$

where $\mathbf{x}=[\,\boldsymbol{\omega}^{\mathrm{T}}\quad\mathbf{F}^{\mathrm{T}}\,]^{\mathrm{T}}$ is the system state vector, $\mathbf{u}=\boldsymbol{\tau}$ is the input torque vector, $\mathbf{L}$ is the energy matrix, $\mathbf{A}(t)$ is the power matrix and $\mathbf{B}$ is the input matrix (Zanasi, 2010). The energy matrix $\mathbf{L}$ and the power matrix $\mathbf{A}(t)$ describe the energy E_s stored in the system and the power P_d dissipated in the system, respectively:

$$E_s=\frac{1}{2}\mathbf{x}^{\mathrm{T}}\mathbf{L}\,\mathbf{x},\qquad P_d=\mathbf{x}^{\mathrm{T}}\mathbf{A}(t)\,\mathbf{x}.\tag{3}$$

The notation "(t)" is adopted in system (2) to denote the system matrices which are supposed to be time-variant, whereas the notation "(t)" is omitted in the system vectors for the sake of brevity. The matrices composing matrix $\mathbf{L}$ are the inertia matrix $\mathbf{J}$ and the stiffness matrix $\mathbf{K}$. The matrices composing matrix $\mathbf{A}(t)$ are the inertia friction matrix $\mathbf{B}_J$, the stiffness friction matrix $\mathbf{B}_K$ and the radii matrix $\mathbf{R}(t)$. The inertia friction matrix $\mathbf{B}_J$ is given by $\mathbf{B}_J=\mathbf{B}_\omega+\mathbf{B}_{\Delta\omega}$, where $\mathbf{B}_\omega$ is the gears friction matrix and $\mathbf{B}_{\Delta\omega}$ is the relative friction matrix. Matrix $\mathbf{B}_J$ includes all and only the friction coefficients acting on the inertial elements, namely the system gears defined within the inertia matrix $\mathbf{J}$. These friction coefficients can be of two different types. The first type are the friction coefficients b_i, for $i\in\mathcal{N}_J$, contained in the first component $\mathbf{B}_\omega$ of $\mathbf{B}_J$ and associated with the rotation of the gears around their own rotation axes. The load torque that inertia J_i experiences due to the presence of the friction coefficient b_i is given by $b_i\,\omega_i$. The second type are the relative friction coefficients b_{ij}, for $ij\in\mathcal{N}_B$, contained in the second component $\mathbf{B}_{\Delta\omega}$ of $\mathbf{B}_J$ and associated with the relative friction existing between the two different gears "i" and "j". The load torque that inertia J_i experiences due to the presence of the friction coefficient b_{ij} is given by $b_{ij}\,(\omega_i-\omega_j)$, whereas the load torque that inertia J_j experiences due to the presence of the friction coefficient b_{ij} is given by $b_{ij}\,(\omega_j-\omega_i)$. The stiffness friction matrix $\mathbf{B}_K$ includes all and only the friction coefficients acting on the elastic elements, namely the system tangential springs defined within the stiffness matrix $\mathbf{K}$. These friction coefficients are denoted as d_{ij}, for $ij\in\mathcal{N}_K$, and represent the friction associated with the tangential springs having stiffness coefficients K_{ij}. The load force generated by the friction coefficient d_{ij} is given by d_{ij} times the product of the "ij" row of matrix $\mathbf{R}(t)$ and the speed vector $\boldsymbol{\omega}$. The output speed vector $\mathbf{y}=\mathbf{B}^{\mathrm{T}}\mathbf{x}=\boldsymbol{\omega}$, the input torque vector and $\mathbf{u}=\boldsymbol{\tau}$, the inertia matrix $\mathbf{J}$ and the gears friction matrix $\mathbf{B}_\omega$ are defined as:

$$\boldsymbol{\omega}=\underset{\mathcal{N}_J}{\overset{i}{\left\|\left[\,\omega_i\,\right]\right\|}},\qquad\boldsymbol{\tau}=\underset{\mathcal{N}_J}{\overset{i}{\left\|\left[\,\tau_i\,\right]\right\|}},\qquad\mathbf{J}=\underset{\mathcal{N}_J}{\overset{i}{\left\|\left[\,J_i\,\right]\right\|}},\qquad\mathbf{B}_\omega=\underset{\mathcal{N}_J}{\overset{i}{\left\|\left[\,b_i\,\right]\right\|}}.\tag{4}$$

The force vector $\mathbf{F}$, the stiffness matrix $\mathbf{K}$ and the stiffness friction matrix $\mathbf{B}_K$ are defined as:

$$\mathbf{F}=\underset{\mathcal{N}_K}{\overset{ij}{\left\|\left[\,F_{ij}\,\right]\right\|}},\qquad\mathbf{K}=\underset{\mathcal{N}_K}{\overset{ij}{\left\|\left[\,K_{ij}\,\right]\right\|}},\qquad\mathbf{B}_K=\underset{\mathcal{N}_K}{\overset{ij}{\left\|\left[\,d_{ij}\,\right]\right\|}}.\tag{5}$$

The reader can easily check that the order of the elements in vectors $\boldsymbol{\omega}$ and $\boldsymbol{\tau}$ and the structure of matrices $\mathbf{J}$ and $\mathbf{B}_\omega$ in (4) are completely defined by the order of the one-digit subscripts i in the ordered set $\mathcal{N}_J$ in (1). Similarly, the order of the elements in vector $\mathbf{F}$ and the structure of matrices $\mathbf{K}$ and $\mathbf{B}_K$ in (5) are completely defined by the order of the two-digit ordered subscripts ij in the ordered set $\mathcal{N}_K$ in (1). The left side of the POG scheme in Fig. 2 clearly shows that the considered system interacts with the other systems through the input vector $\boldsymbol{\tau}$, containing the external torques, and through the output vector $\boldsymbol{\omega}$, containing the gears angular speeds. The input torques in $\boldsymbol{\tau}$ are either *controlled torques* or *load torques*. As an example, if the considered gear system was a planetary gear set to be employed in an HEV (Tebaldi & Zanasi, 2021), the *controlled torques* in $\boldsymbol{\tau}$ would be the electric machine and the internal combustion engine motive torques, whereas the *load torque* would be the transmission load torque. If the considered gear system was a differential to be employed in a transmission system, see Section 5, the *controlled torque* in $\boldsymbol{\tau}$ would be the transmission shaft motive torque, whereas the *load torques* would be the left and right wheel torques. Furthermore, from (2), note that the system state vector $\mathbf{x}$ contains the force vector $\mathbf{F}$. Consequently, the engineer can freely apply any control law to generate the *controlled torques*, and thus simulate all possible operating conditions by reading the resulting speed and force vectors $\boldsymbol{\omega}$ and $\boldsymbol{F}$. These two examples highlight the versatility of the proposed model, which can describe any time-variant

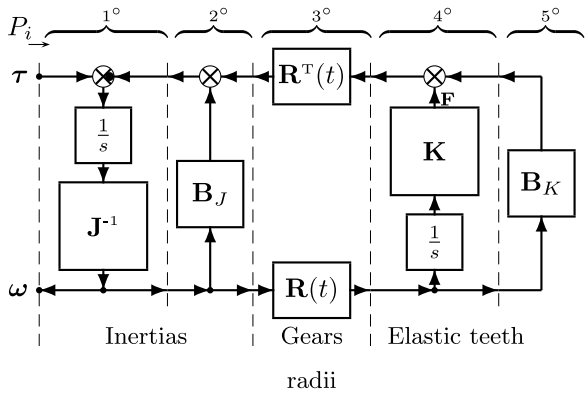

Fig. 2. General POG scheme of time-variant gear systems.

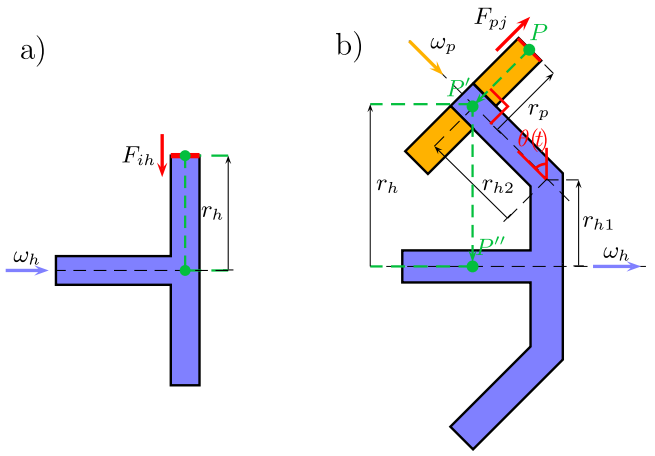

Fig. 3. *Effective radii* r_h: (a) Direct contact; (b) Indirect contact.

or time-invariant gear system having parallel or oblique rotation axes, working in any desired operating condition.

The only two matrices which are not defined yet are the relative friction matrix $\mathbf{B}_{\Delta\omega}$ and the radii matrix $\mathbf{R}(t)$. The former accounts for the relative friction between couples of gears in the system. Matrix $\mathbf{B}_{\Delta\omega}$ can be effectively and systematically computed using the Algorithm 2 in Appendix A. The radii matrix $\mathbf{R}(t)$ contains the radii of the system, see Section 4.1, which determine the interaction between the gears and the tangential springs in the considered gear system. The radii within matrix $\mathbf{R}(t)$ are completely determined by the structure of the considered gear system. The algorithm for the systematic computation of matrix $\mathbf{R}(t)$ is reported in the next Section 4.1.

The state–space model (2) can be straightforwardly implemented in the Simulink environment using the equivalent block scheme shown in Fig. 2. The two fundamental blocks in POG schemes (Zanasi, 2010) are the elaboration and connection blocks, modeling physical elements and energy conversions, respectively. In Fig. 2, the 1° block models the gears inertial dynamics. The 2° block introduces the gears viscous and relative frictions. The 3° block describes the energy conversion between the rotational and translational mechanical domains. The operation $\mathbf{R}(t)\boldsymbol{\omega}$ generates a tangential speeds difference vector charging the tangential springs. As an example let us refer to Fig. 1, where the difference between $v_a = \omega_a r_a$ and $v_b = \omega_b r_b$ charges the tangential spring K_{ab}, thus generating the force F_{ab} acting on the tangential direction with respect to the two gears a and b. The operation $\mathbf{R}(t)^T \boldsymbol{F}$ (neglecting the friction coefficients in matrix $\mathbf{B}_K$ for the purpose of this explanation) generates a load torques vector applied to the gears as a result of their elastic coupling. The 4° block describes the gears elastic contact points. Finally, the 5° block introduces the tangential springs friction coefficients. From the POG block scheme in Fig. 2, the reader can verify that the radii matrix $\mathbf{R}(t)$ is located inside the connection block denoted as "Gears radii", meaning that it physically describes the energy conversions taking place within the system. In the considered case, the energy conversions are those between the physical elements in the mechanical rotational domain, i.e. the system gears, and those in the mechanical translational domain, i.e. the contact tangential springs. In the generalization provided in this paper, it is assumed that the interactions between two or more gears change in time, meaning that one or more radii are time-variant.

4.1. Algorithm 1: calculation of the radii matrix $\mathbf{R}(t)$

Let $r_{ij,h}(t)$ denote the generic coefficient of matrix $\mathbf{R}(t) = [r_{ij,h}(t)]$, where $ij \in \mathcal{N}_K$ and $h \in \mathcal{N}_J$, see (1). Coefficient $r_{ij,h}(t)$ links the angular speed ω_h of gear h to the tangential speed of one of the two terminals of the tangential spring K_{ij}.

Property 1. *The generic coefficient* $r_{ij,h}(t)$ *of the radii matrix* $\mathbf{R}(t)$ *can be computed as follows:*

$$r_{ij,h}(t) = S_{F_{ij}}\, S_{\omega_h}\, r_h(t). \tag{6}$$

Let us describe the meaning of the terms in (6) with reference to the example reported in Fig. 3. Note that the horizontal colored arrows " $\rightarrow$ *" and "* $\rightarrow$ *", shown in Fig. 3, and similarly the horizontal colored arrows in the other gear systems representations following in this paper, highlight the positive direction of the gears rotation axes.*

(a) $r_h(t)$ *is the "effective radius" which links the angular speed* ω_h *to the tangential force* F_{ij}*. Under the hypothesis that the gears rotation axes are all located on the same plane, we distinguish the two cases: (1) if the angular speed* ω_h *directly affects the force* F_{ij}*, see the direct contact of Fig. 3.a, then the effective radius* $r_h(t)$ *coincides with the radius of the gear which links velocity* ω_h *to force* F_{ij}*; (2) if the angular speed* ω_h *affects the force* F_{ij} *through an intermediate gear "p", see the indirect contact of Fig. 3.b as an example, then the effective radius* $r_h(t)$ *is computed as follows: the central point* P *of force* F_{ij} *has to be orthogonally projected on the rotation axis of the angular speed* ω_p *associated with the intermediate gear "p", thus generating point* P'*, see Fig. 3.b. The effective radius* $r_h(t)$ *is given by the distance between the resulting projected point* P' *and the rotation axis of* ω_h*, namely distance* $P' - P''$*. In the scenario shown in Fig. 3.b, it is* $r_h(t) = r_{h1} + r_{h2}\cos\theta(t)$*.* Note that the described indirect contact case is a generalization of the one depicted in Zanasi and Tebaldi (2020a)-Fig. 5.b, *where the angle* $\theta(t)$ *was supposed to be constant and equal to* $\pi/2$*, i.e. the rotation axes of the two involved angular speeds* ω_h *and* ω_p *were supposed to be parallel.*

(b) $S_{F_{ij}}$ *is the sign related to the positive orientation of vector* F_{ij}*:*

$$S_{F_{ij}} = \begin{cases} 1 & \text{if } i = h \text{ (direct) or } i = p \text{ (indirect)}, \\ -1 & \text{if } j = h \text{ (direct) or } j = p \text{ (indirect)}. \end{cases}$$

As an example, $S_{F_{ih}} = -1$ *in Fig. 3.a and* $S_{F_{pj}} = 1$ *in Fig. 3.b.*

(c) S_{ω_h} *is the sign related to the positive orientation of the velocity vector* ω_h*:*

$$S_{\omega_h} = \begin{cases} 1 & \text{if force } F_{ij} \text{ is on the left of vector } \omega_h, \\ -1 & \text{if force } F_{ij} \text{ is on the right of vector } \omega_h. \end{cases}$$

The left and right sides of vector ω_h *are determined by moving along the positive direction of vector* ω_h*.*

Remark 1. The proposed algorithm represents a generalization of the Algorithm 1 proposed in Zanasi and Tebaldi (2020a) introducing the following important new features: the generic coefficient $r_{ij,h}(t)$ of the radii matrix $\mathbf{R}(t)$ *can now be a function of time*. This is thanks

to the fact that, in the indirect contact case, the new version of the algorithm allows the angle between the rotation axes of the two involved angular speeds ω_h and ω_p *to be such that the two rotation axes are no longer constrained to be oblique, but their position can now be varying with time*. Note that, in the previous version of Algorithm 1 given in the previous work, the angle between the rotation axes of the two involved angular speeds ω_h and ω_p in the indirect contact case was always constant and giving parallel rotation axes, thus excluding the oblique and time-variant cases. The new generalization allows to use the proposed systematic methodology not only for the modeling of planetary gear sets, as it was in the previous work, but its use is now extended to the modeling of a large variety of complex gear systems as well, including half and full toroidal variators, vehicle differentials, and any other type of system including bevel gearing systems having different shaft operating angles between the gear shafts.

4.2. Reduced rigid model

The full model (2) is suitable for accurately simulating the system including the gears elastic coupling, but is not suitable for fixed-step simulations needed for real-time execution. This is due to the tangential springs fast dynamics, which would cause the step size to be very low, thus significantly increasing the simulation time. A solution for fixed-step simulations is to use a reduced rigid model assuming rigid connections between the system gears, which can be systematically computed as described in this section. When an eigenvalue of the energy matrix $\mathbf{L}$ tends to zero, the system model degenerates to a lower dimension system (Zanasi, 2010), and the reduced model can be obtained by applying a proper congruent transformation $\mathbf{x} = \mathbf{T}_1\,\mathbf{x}_1$, where $\mathbf{x}$ is the state vector of the original full model, $\mathbf{x}_1$ is the state vector of the new reduced model and $\mathbf{T}_1$ is a proper rectangular matrix. Let us assume all the coefficients K_{ij}, for $ij \in \mathcal{N}_K$, within the stiffness matrix $\mathbf{K}$ contained in the energy matrix $\mathbf{L}$ in (2) to tend to infinity. From the second equation in (2), one obtains:

$$\mathbf{R}(t)\,\boldsymbol{\omega} = \mathbf{0}. \tag{7}$$

Remark 2. In order for the model to be feasible, system (7) must exhibit static constraints between the n_J angular speeds ω_i leaving at least one degree of freedom. From a mathematical point of view, this means that $n_J > n_K$ and $\text{rank}(\mathbf{R}(t)) = n_K$. Under these conditions, system (7) can be used to express n_K angular speeds ω_i as a function of the remaining $n_J - n_K$ angular speeds, which compose the state vector $\mathbf{x}_1 = \boldsymbol{\omega}_\mathbf{1}$ of the reduced model.

By rewriting the n_K equations in system (7) in a matrix form, and including $n_J - n_K$ identities, one can build a matrix $\mathbf{Q}_1(t)$, which expresses the n_J angular speed of the considered gear system as a function of the $n_J - n_K$ angular speeds that remain in the reduced state vector $\mathbf{x}_1$ assuming rigid gears connections. The original state vector $\mathbf{x}$ in (2) can therefore be expressed as a function of $\mathbf{x}_1$ by means of the following time-variant congruent transformation matrix $\mathbf{T}_1(t)$:

$$\underbrace{\begin{bmatrix}\boldsymbol{\omega}\\ \mathbf{F}\end{bmatrix}}_{\mathbf{x}} = \underbrace{\begin{bmatrix}\mathbf{Q}_1(t)\\ \mathbf{0}\end{bmatrix}}_{\mathbf{T}_1(t)} \underbrace{\mathbf{x}_1}_{\boldsymbol{\omega}_\mathbf{1}}, \qquad \text{where} \qquad \boldsymbol{\omega} = \mathbf{Q}_1(t)\,\mathbf{x}_1 \tag{8}$$

and $\mathbf{x}_1 = \boldsymbol{\omega}_\mathbf{1}$ contains the angular speeds in the reduced model. By applying $\mathbf{x} = \mathbf{T}_1(t)\,\mathbf{x}_1$ to system (2), one obtains the following reduced state space time-variant model:

$$\mathbf{L}_1(t)\,\dot{\mathbf{x}}_1 + \mathbf{N}_1(t)\,\mathbf{x}_1 = \mathbf{A}_1(t)\,\mathbf{x}_1 + \mathbf{B}_1(t)\,\mathbf{u}, \tag{9}$$

where matrices $\mathbf{L}_1(t)$, $\mathbf{N}_1(t)$, $\mathbf{A}_1(t)$ and $\mathbf{B}_1(t)$ are given by:

$$\begin{cases}\mathbf{L}_1(t) = \mathbf{T}_1(t)^\mathrm{T}\mathbf{L}\,\mathbf{T}_1(t) = \mathbf{Q}_1(t)^\mathrm{T}\mathbf{J}\,\mathbf{Q}_1(t),\\ \mathbf{N}_1(t) = \mathbf{T}_1(t)^\mathrm{T}\mathbf{L}\,\dot{\mathbf{T}}_1(t) = \mathbf{Q}_1(t)^\mathrm{T}\mathbf{J}\,\dot{\mathbf{Q}}_1(t),\\ \mathbf{A}_1(t) = \mathbf{T}_1(t)^\mathrm{T}\mathbf{A}\,\mathbf{T}_1(t) = -\mathbf{Q}_1(t)^\mathrm{T}\mathbf{B}_J\mathbf{Q}_1(t),\\ \mathbf{B}_1(t) = \mathbf{T}_1(t)^\mathrm{T}\mathbf{B} = \mathbf{Q}_1^\mathrm{T}(t).\end{cases} \tag{10}$$

Remark 3. The time variance of the original model (2) was supposed to be contained only in matrix $\mathbf{R}(t)$. This choice was dictated by the fact that matrix $\mathbf{R}(t)$ contains the *effective radii* of the gears, see Section 4.1. Assuming that an effective radius can be time-variant means assuming that the system physical configuration can change. An example is given in the full toroidal variator of Section 6, where the time variance of two elements in matrix $\mathbf{R}(t)$ determines a variation of the tilt angle $\theta(t)$ of the full toroidal variator rollers. The matrices $\mathbf{L}_1(t)$, $\mathbf{N}_1(t)$, $\mathbf{A}_1(t)$ and $\mathbf{B}_1(t)$ of the reduced model (9) are all time-variant, since they are obtained from the original ones applying the time-variant transformation $\mathbf{T}_1(t)$, as in (10).

4.3. Calculation of the force vector F

The reduced state vector $\mathbf{x}_1$ of system (9) no longer contains the force vector $\mathbf{F}$, which was instead present in the original state vector $\mathbf{x}$ of system (2). However, the time behavior of vector $\mathbf{F}$ can still be computed in the reduced system (9), as shown in Property 2.

Property 2. *The time behavior of the force vector* $\mathbf{F}$ *can be obtained from the reduced state vector* $\mathbf{x}_1$ *and the input vector* $\mathbf{u} = \boldsymbol{\tau}$ *of the reduced system* (9) *using the relation:*

$$\mathbf{F} = \mathbf{M}_p(t)\left[\boldsymbol{\tau} - \left(\mathbf{B}_J\mathbf{Q}_1(t) + \mathbf{J}\dot{\mathbf{Q}}_1(t)\right)\mathbf{x}_1\right], \tag{11}$$

with $\mathbf{M}_p(t) = \left(\mathbf{R}(t)\mathbf{J}^{-1}\mathbf{R}^T(t)\right)^{-1}\mathbf{R}(t)\mathbf{J}^{-1}$. *The input torque vector* $\boldsymbol{\tau}$, *the inertia matrix* $\mathbf{J}$, *the inertia friction matrix* $\mathbf{B}_J$ *and the radii matrix* $\mathbf{R}(t)$ *have been defined in Section 4 right after the introduction of system* (2). *Matrix* $\mathbf{Q}_1(t)$ *within the transformation matrix* $\mathbf{T}_1(t)$ *and the reduced state vector* $\mathbf{x}_1$ *have been introduced in* (8) *when deriving the reduced model* (9). *The proof of Property 2 is given in Appendix B.*

5. Differential

5.1. Differential with non-perpendicular shafts

Let us consider the differential with non-perpendicular gear shafts shown in Fig. 4. Note that the red lines "▬" located at the contact points between the system gears denote the presence of the tangential springs. This system can be modeled using the dynamic model given in (2), the POG scheme shown in Fig. 2, and the systematic procedure presented in Section 4, where:

$$\begin{cases}\mathcal{N}_J = \{a, b, c, d, e, f, g\}, & n_J = \dim(\mathcal{N}_J) = 7,\\ \mathcal{N}_K = \{ag, cb, dc, de, ef\}, & n_K = \dim(\mathcal{N}_K) = 5,\\ \mathcal{N}_B = \{\}, & n_B = \dim(\mathcal{N}_B) = 0.\end{cases} \tag{12}$$

Note: the user is free to change set $\mathcal{N}_B$ in (12) at will, in order to simulate different types of relative friction conditions. From $\mathcal{N}_J$ in (12), the output speed vector $\boldsymbol{\omega}$, the input torque vector $\boldsymbol{\tau}$, the inertia matrix $\mathbf{J}$ and the gears friction matrix $\mathbf{B}_\omega$ can be computed using (4). From $\mathcal{N}_K$ in (12), the force vector $\mathbf{F}$, the stiffness matrix $\mathbf{K}$ and the stiffness friction matrix $\mathbf{B}_K$ can be computed using (5). Matrix $\mathbf{B}_{\Delta\omega} = \mathbf{0}$ according to set $\mathcal{N}_B$ in (12) and using Algorithm 2 in Appendix A. Matrix $\mathbf{R}$ can be automatically computed using the Algorithm 1 presented in Section 4.1:

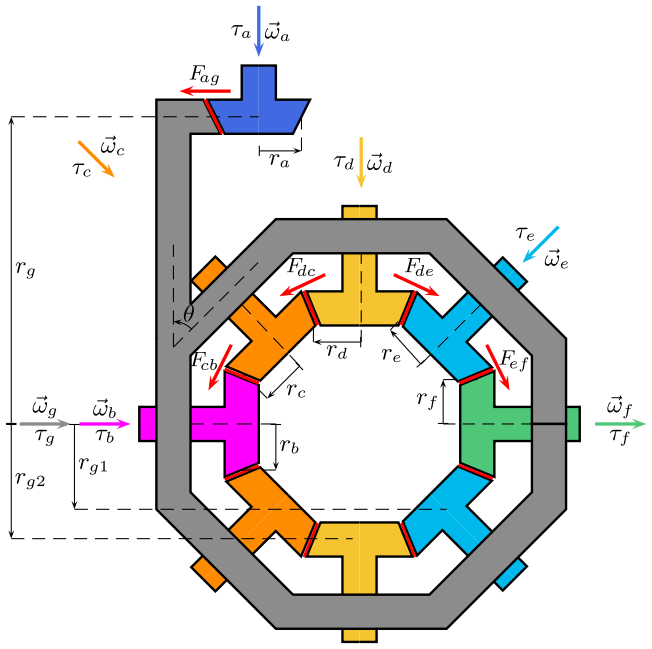

Fig. 4. Differential structure with non-perpendicular gear shafts.

$$\mathbf{R}=\begin{array}{c} \\ ag \\ cb \\ dc \\ de \\ ef \end{array}\begin{array}{c} \begin{array}{ccccccc} a & b & c & d & e & f & g \end{array} \\ \begin{bmatrix} -r_a & 0 & 0 & 0 & 0 & 0 & -r_g \\ 0 & -r_b & -r_c & 0 & 0 & 0 & r_{g1} \\ 0 & 0 & -r_c & -r_d & 0 & 0 & r_{g2}-r_{g1} \\ 0 & 0 & 0 & r_d & r_e & 0 & r_{g2}-r_{g1} \\ 0 & 0 & 0 & 0 & r_e & -r_f & r_{g1} \end{bmatrix} \end{array}, \tag{13}$$

where $r_{g1} = r_f + r_e\cos\theta = r_b + r_c\cos\theta$ and $r_{g2} = r_b + 2r_c\cos\theta = r_f + 2r_e\cos\theta$. Note that parameter θ in Fig. 4 is a constant angle. When the stiffness coefficients within the stiffness matrix $\mathbf{K}$ tend to infinity, that is when $\mathbf{K} \to \infty$, from (2) one can write the state vector $\mathbf{x}$ as a function of the chosen reduced state vector $\mathbf{x}_1$ using the congruent transformation in (8), where:

$$\mathbf{Q}_1=\begin{bmatrix} -\frac{r_b r_g}{r_a(r_b+r_f)} & -\frac{r_f r_g}{r_a(r_b+r_f)} \\ 1 & 0 \\ -\frac{r_b(r_f-r_c\cos\theta)}{r_c(r_b+r_f)} & \frac{r_f(r_b+r_c\cos\theta)}{r_c(r_b+r_f)} \\ \frac{r_b r_f}{r_d(r_b+r_f)} & -\frac{r_b r_f}{r_d(r_b+r_f)} \\ -\frac{r_b(r_f+r_e\cos\theta)}{r_e(r_b+r_f)} & \frac{r_f(r_b-r_e\cos\theta)}{r_e(r_b+r_f)} \\ 0 & 1 \\ \frac{r_b}{r_b+r_f} & \frac{r_f}{r_b+r_f} \end{bmatrix}, \qquad \mathbf{x}_1=\begin{bmatrix}\omega_b \\ \omega_f\end{bmatrix}. \tag{14}$$

The resulting reduced system is structured as in (9), whereas the system matrices can be computed as in (10). Since matrix $\mathbf{Q}_1$ is constant, from (10) it follows $\mathbf{N}_1 = \mathbf{0}$ in the considered reduced system.

Matlab/Simulink files allowing to perform simulations of the proposed differential structure are provided in the supplementary material in Appendix C within the folder named "`Non_Perpendicular_Differential`". The unified Simulink implementation of the full and reduced models is named "`Unified_Scheme_FULL_RED_SLX.slx`". The scripts launching the simulation of the full and reduced models are named "`NP_Differential_Full.m`" and "`NP_Differential_Reduced.m`", respectively.

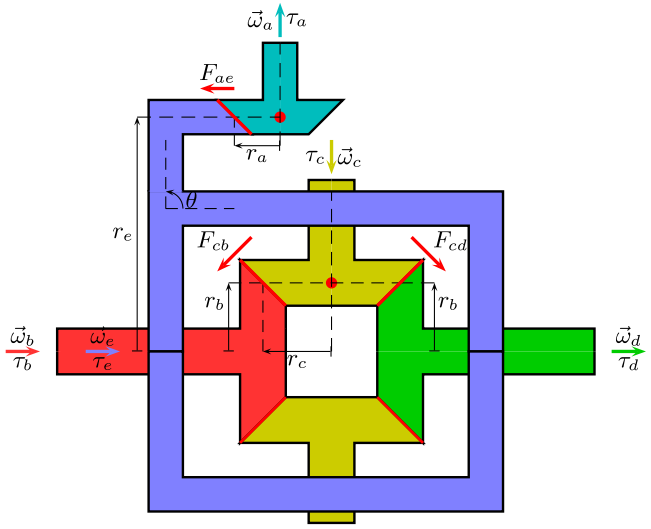

Fig. 5. Structure of the considered vehicle differential.

5.2. Differential with perpendicular shafts: Modeling

Let us consider the differential shown in Fig. 5. This system can be modeled using (2) and following the systematic procedure presented in Section 4. For the considered system, it is:

$$\begin{cases} \mathcal{N}_J = \{a,\, b,\, c,\, d,\, e\}, & n_J = \dim(\mathcal{N}_J) = 5, \\ \mathcal{N}_K = \{ae,\, cb,\, cd\}, & n_K = \dim(\mathcal{N}_K) = 3, \\ \mathcal{N}_B = \{eb,\, ed\}, & n_B = \dim(\mathcal{N}_B) = 2. \end{cases} \tag{15}$$

From $\mathcal{N}_J$ in (15), the output speed vector $\boldsymbol{\omega}$, the input torque vector $\boldsymbol{\tau}$, the inertia matrix $\mathbf{J}$ and the gears friction matrix $\mathbf{B}_\omega$ can be computed using (4). From $\mathcal{N}_K$ in (15), the force vector $\mathbf{F}$, the stiffness matrix $\mathbf{K}$ and the stiffness friction matrix $\mathbf{B}_K$ can be computed using (5). By referring to set $\mathcal{N}_B$ and using the Algorithm 2 in Appendix A, one can systematically build the following relative friction matrix $\mathbf{B}_{\Delta\omega}$:

$$\mathbf{B}_{\Delta\omega}=\begin{array}{c} \\ a \\ b \\ c \\ d \\ e \end{array}\begin{array}{c} \begin{array}{ccccc} a & b & c & d & e \end{array} \\ \begin{bmatrix} 0 & 0 & 0 & 0 & 0 \\ 0 & b_{eb} & 0 & 0 & -b_{eb} \\ 0 & 0 & 0 & 0 & 0 \\ 0 & 0 & 0 & b_{ed} & -b_{ed} \\ 0 & -b_{eb} & 0 & -b_{ed} & b_{eb}+b_{ed} \end{bmatrix} \end{array}. \tag{16}$$

The relative friction coefficients b_{eb} and b_{ed} within matrix $\mathbf{B}_{\Delta\omega}$ account for the linear relative friction between the case (element e) and the left axle shaft (element b), and between the case and the right axle shaft (element d), see Fig. 5. The radii matrix $\mathbf{R}$ is obtained using Algorithm 1 in Section 4.1:

$$\mathbf{R}=\begin{array}{c} \\ ae \\ cb \\ cd \end{array}\begin{array}{c} \begin{array}{ccccc} a & b & c & d & e \end{array} \\ \begin{bmatrix} r_a & 0 & 0 & 0 & -r_e \\ 0 & -r_b & -r_c & 0 & r_b \\ 0 & 0 & r_c & -r_b & r_b \end{bmatrix} \end{array}. \tag{17}$$

For the considered case study, parameter θ is a constant angle. This differential can be seen as a particular case of the more general one shown in Fig. 4 with $\theta = \pi/2$, i.e. the two elements encircled in red in (17) follow from $r_b + r_c\cos\theta = r_b$. When the stiffness coefficients within the stiffness matrix $\mathbf{K}$ tend to infinity, that is when $\mathbf{K} \to \infty$, using (2), (4), (5) and (15), one can write the state vector $\mathbf{x}$ as a function of the chosen reduced state vector $\mathbf{x}_1 = [\omega_b \;\; \omega_d]^{\mathrm{T}}$. In this case, matrix $\mathbf{Q}_1$ in

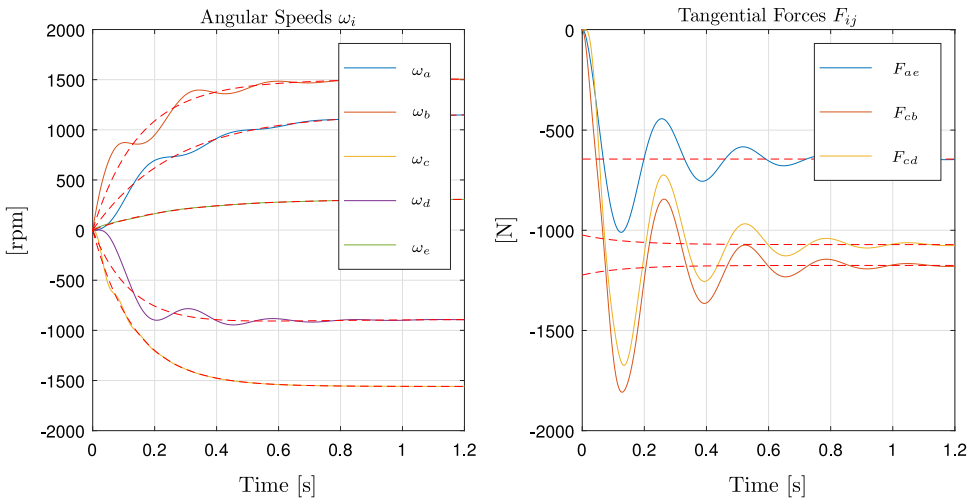

Fig. 6. Simulation of the vehicle differential: full (colored characteristics) and reduced (dashed characteristics) models.

Table 1
Differential: parameters.

$\theta = \pi/2$ rad	$J_c = J_e = 5 \cdot 10^{-3}$ kg m^2, $b_c = b_e = 2 \cdot 10^{-3}$ Nm/rpm
$J_a = J_b = J_d = 5 \cdot 10^{-2}$ kg m^2, $b_a = b_b = b_d = 2 \cdot 10^{-2}$ Nm/rpm	
$r_a = 36$ mm, $r_b = 39$ mm, $r_c = 30$ mm, $r_e = 135$ mm, $d_{ae} = d_{cb} = d_{cd} = 70$ N s/m	
$K_{ae} = K_{cb} = K_{cd} = 20$ kN/m, $b_{eb} = b_{ed} = 2 \cdot 10^{-2}$ Nm/rpm	

(8) is given by:

$$\mathbf{Q}_1 = \begin{bmatrix} \frac{r_e}{2r_a} & \frac{r_e}{2r_a} \\ 1 & 0 \\ -\frac{r_b}{2r_c} & \frac{r_b}{2r_c} \\ 0 & 1 \\ \frac{1}{2} & \frac{1}{2} \end{bmatrix}. \tag{18}$$

The resulting reduced system has the structure given in (9) and (10). Note that, since matrix $\mathbf{Q}_1$ is constant in (10), $\mathbf{N}_1 = \mathbf{0}$ from (10).

5.3. Differential with perpendicular shafts: Simulation

The differential reported in Fig. 5 has been simulated using the system parameters given in Table 1, starting from zero initial conditions and applying an input torque $\tau_b = 100$ Nm to gear b. The resulting angular speeds ω_i and tangential forces F_{ij}, for $i \in \mathcal{N}_J$ and $ij \in \mathcal{N}_K$, are reported in Fig. 6. In the figure, the colored characteristics come from the simulation of the full model, whereas the red dashed characteristics come from the simulation of the reduced model. Note that the time behavior of the tangential forces F_{ij} of the reduced system has been computed using the relation presented in (11). The matching between the time behaviors given by the two models highlights the effectiveness of the reduced model, as well as the effectiveness of Eq. (11). The Matlab/Simulink files allowing to perform the described simulation are provided in the supplementary material in Appendix C within the folder named "`Differential`". The unified Simulink implementation of the full and reduced models is named "`Unified_Scheme_FULL_RED_SLX.slx`". The scripts launching the simulation of the full and reduced models are named "`Differential_Full.m`" and "`Differential_Reduced.m`", respectively.

6. Full toroidal variator

6.1. Modeling

The full toroidal variator shown in Fig. 7 was modeled in Zanasi et al. (2014) using the POG technique. A much more effective and less prone to mistakes approach for modeling it is given by the systematic methodology presented in this paper, as shown in the following. The considered system can be modeled using the dynamic model given in (2), where:

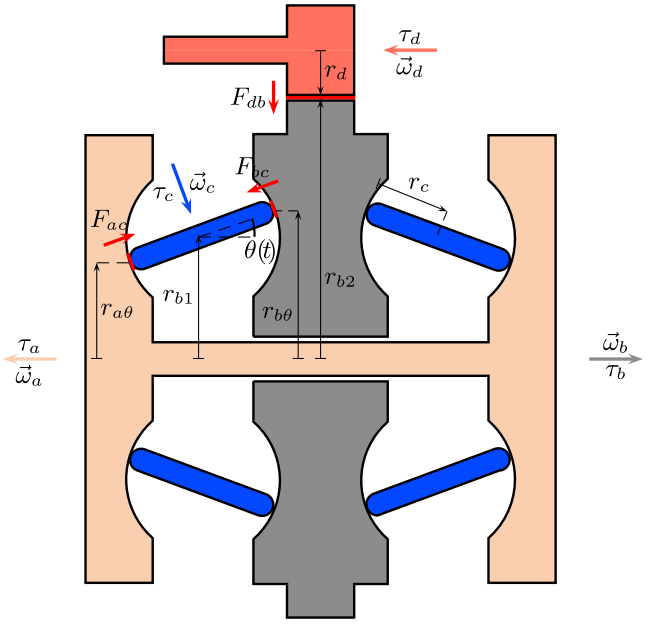

Fig. 7. Structure of the considered full toroidal variator.

$$\begin{cases} \mathcal{N}_J = \{a, b, c, d\}, & n_J = \dim(\mathcal{N}_J) = 4, \\ \mathcal{N}_K = \{bc, ac, db\}, & n_K = \dim(\mathcal{N}_K) = 3, \\ \mathcal{N}_B = \{\}, & n_B = \dim(\mathcal{N}_B) = 0. \end{cases} \tag{19}$$

From $\mathcal{N}_J$ in (19), the output speed vector $\boldsymbol{\omega}$, the input torque vector $\boldsymbol{\tau}$, the inertia matrix $\mathbf{J}$ and the gears friction matrix $\mathbf{B}_\omega$ can be computed using (4). From $\mathcal{N}_K$ in (19), the force vector $\mathbf{F}$, the stiffness matrix $\mathbf{K}$ and the stiffness friction matrix $\mathbf{B}_K$ can be computed using (5).

Using Algorithm 1 in Section 4.1, the radii matrix $\mathbf{R}(t)$ is:

$$\begin{matrix} \\ bc \\ ac \\ db \end{matrix} \mathbf{R}(t) = \begin{matrix} \begin{bmatrix} a & b & c & d \end{bmatrix} \\ \begin{bmatrix} 0 & r_{b\theta} & -r_c & 0 \\ -r_{a\theta} & 0 & r_c & 0 \\ 0 & -r_{b2} & 0 & r_d \end{bmatrix} \end{matrix}. \tag{20}$$

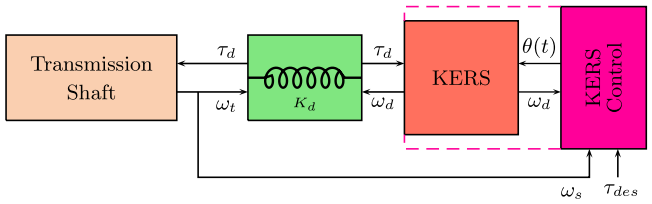

Fig. 8. Considered automotive system with KERS.

In this case, the time-variant matrix $\mathbf{R}(t)$ is a function of the time-variant angle $\theta(t)$, meaning that the energy conversion taking place between some system gears and some tangential springs varies with time, see Fig. 2. The terms $r_{b\theta}$ and $r_{a\theta}$ in matrix $\mathbf{R}(t)$ are given by: $r_{b\theta} = r_{b1} + r_c \sin\theta(t)$ and $r_{a\theta} = r_{b1} - r_c \sin\theta(t)$, respectively.

When the stiffness coefficients within the stiffness matrix $\mathbf{K}$ tend to infinity, that is when $\mathbf{K} \to \infty$, from (2), (4), (5) and (19), one can write the state vector $\mathbf{x}$ as a function of the chosen reduced state vector $\mathbf{x}_1 = \omega_d$ using (8), where matrix $\mathbf{Q}_1(t)$ is:

$$\mathbf{Q}_1(t) = \begin{bmatrix} \frac{r_d(r_{b1}+r_c\sin\theta(t))}{r_{b2}(r_{b1}-r_c\sin\theta(t))} \\ \frac{r_d}{r_{b2}} \\ \frac{r_d(r_{b1}+r_c\sin\theta(t))}{r_{b2}r_c} \\ 1 \end{bmatrix} = \begin{bmatrix} R_{a\theta} \\ R_b \\ R_{c\theta} \\ R_d \end{bmatrix} = \begin{bmatrix} \frac{\omega_a}{\omega_d} \\ \frac{\omega_b}{\omega_d} \\ \frac{\omega_c}{\omega_d} \\ 1 \end{bmatrix}. \tag{21}$$

The resulting reduced system has the structure given in (9) and (10). Note that, since matrix $\mathbf{Q}_1(t)$ is time-variant, in this case matrix $\mathbf{N}_1(t)$ is a non-zero time-variant matrix. In this case, the reduced system (9) can also be rewritten as a scalar time-variant differential equation:

$$J(t)\,\dot{\omega}_d + N(t)\,\omega_d = A(t)\,\omega_d + \tau_d, \tag{22}$$

where matrices $\mathbf{L}_1(t)$, $\mathbf{N}_1(t)$, $\mathbf{A}_1(t)$ reduce to the scalar time-variant parameters $J(t)$, $N(t)$, $A(t)$, respectively, whereas matrix $\mathbf{B}_1(t)$ reduces to the constant 1.

6.2. Control

One of the main applications of the full toroidal variator in the automotive world is KERS (Kinetic Energy Recovery System). In this case, this device is placed within the vehicle architecture and is used as a temporary energy storage device to recover kinetic energy under certain vehicle operating conditions (e.g. during braking). Let us consider the case study reported in Fig. 8, where the full toroidal variator acting as a KERS is connected to the vehicle transmission shaft, with angular speed ω_t, through a torsional spring having the following dynamics: $\tau_d = K_d/s\,(\omega_t - \omega_d)$.

The "KERS Control" block in Fig. 8 acts on the position $\theta(t)$ of the KERS rollers to force the torque τ_d to track the desired torque τ_{des}, which will be provided by a higher order control of the vehicle architecture (Energy Management System). The structure of the "KERS Control" is shown in Fig. 9. The output variable $\theta(t)$ of the KERS Control is obtained by using the integral control $\dot{\theta}(t) = K_\theta(\Delta\tau - K_w\Delta_\omega)$, where $\Delta\tau = \tau_{des} - \tilde{\tau}_d$ and $\Delta_\omega = \omega_t - \omega_d$. Variable $\tilde{\tau}_d$ is an estimation of the torque τ_d that the torsional spring applies to the KERS. The kinetic energy $E_s = E(\omega_d, \theta(t))$ stored within the KERS and the power P_d dissipated within the KERS can be computed as in (3), with $\mathbf{L} = J(\theta)$, $\mathbf{A}(t) = A(\theta(t))$ and $\mathbf{x} = \omega_d$. The τ_d estimator is based on $E(\omega_d, \theta)$, as follows. The time-derivative of $E(\omega_d, \theta(t))$ is equal to the sum of the power flow $\tau_d\,\omega_d$ entering into the KERS and of the dissipated power $P_d = A(\theta(t))\omega_d^2$:

$$\dot{E} = \tau_d\,\omega_d + A(\theta(t))\omega_d^2 \qquad \to \qquad \tilde{\tau}_d = \frac{\dot{E}}{\omega_d} - A(\theta(t))\,\omega_d, \tag{23}$$

where $\tilde{\tau}_d$ is an estimation of torque τ_d coming from the numerical time-derivative $\dot{E}$.

Table 2
Full toroidal variator and KERS Control: parameters.

$J_a = 0.179$ kg m^2, $J_b = 1.8 \cdot 10^{-3}$ kg m^2, $J_c = 0.756 \cdot 10^{-3}$ kg m^2
$J_d = 0.026$ kg m^2, $b_a = 0.325 \cdot 10^{-3}$ Nm/rpm, $b_b = 0.55 \cdot 10^{-3}$ Nm/rpm
$b_c = 0.475 \cdot 10^{-3}$ Nm/rpm, $b_d = 0.265 \cdot 10^{-3}$ Nm/rpm
$r_{b1} = 34.3$ mm, $r_{b2} = 51.5$ mm, $r_c = 27.5$ mm, $r_d = 17.2$ mm
$K_{bc} = K_{ac} = 400$ kN/m, $K_{db} = 750$ kN/m, $d_{bc} = d_{ac} = d_{db} = 10^3$ N s/m
$K_d = 30 \cdot 10^3$ Nm/rad, $K_\theta = 10$, $K_w = 10$

6.3. Simulation

Let us perform a simulation with reference to the automotive case study in Fig. 8. The proposed control has been developed based on the reduced full toroidal variator model (22). The full toroidal variator and KERS control parameters are reported in Table 2. The transmission shaft (see Fig. 8) is supposed to be rotating at a constant speed $\omega_t = 1000$ rpm, which is also the initial condition of the "d" inertial element of the full toroidal variator (see Fig. 7). The time-derivative $\dot{E}$ is computed by using the response of the transfer function $s/(10^{-4}s + 1)$ on the stored energy E. For the analyzed fraction of driving cycle, the energy management system is supposed to be requiring the desired torque τ_{des} plotted in red dashed line in the second subplot of Fig. 10. The simulation results are shown in Figs. 10 and 11. The first subplot of Fig. 10 shows the transmission shaft speed ω_t and the full toroidal variator speed ω_d. The second subplot of Fig. 10 shows the desired torque τ_{des}, the actual torque τ_d and the estimated torque $\tilde{\tau}_d$. The third and fourth subplots of Fig. 10 show the controlled tilt angle $\theta(t)$ enforced by the KERS control and the energy $E(\omega_d, \theta(t))$ stored within the KERS. The good superposition between speeds ω_t and ω_d, together with the good superposition between torques τ_{des} and τ_d, proves the effectiveness of the proposed KERS control. The good superposition between torques $\tilde{\tau}_d$ and τ_d proves the effectiveness of the proposed torque estimator. Fig. 11 shows the full toroidal variator angular speeds ω_i and tangential forces F_{ij}, for $i \in \mathcal{N}_J$ and $ij \in \mathcal{N}_K$.

Matlab/Simulink files allowing to perform additional simulations of the full toroidal variator are provided in the supplementary material in Appendix C within the folder named "`Full_Toroidal _Variator`". The unified Simulink implementation of the full and reduced models is named "`Unified_Scheme_FULL_RED_SLX.slx`". The scripts launching the simulation of the full and reduced models are named "`Full_Toroidal_Variator_Full.m`" and "`Full_Toroidal_Variator_Reduced.m`", respectively.

7. Contributions with respect to the literature

To the best of our knowledge, *there is no unified systematic methodology* allowing to model any time-variant gear system composed of planetary, parallel and oblique rotation axes. Therefore, the comparison with other approaches employed in the literature needs to be addressed on a case-to-case basis.

(1) Differential. Let us refer to the Matlab/Simulink open differential model (S., 0000a). The model obtained using the proposed systematic modeling approach offers the following benefits compared to the one made available by the Matlab/Simulink tools: (a) it accounts for the inertia of the rotating external case and of the elements attached to it (J_e and J_c, respectively, with reference to Fig. 5) and for the friction associated with them; (b) it allows to insert relative frictions between gears; (c) it allows to obtain both a fully elastic model and a reduced order model; (d) the same methodology can be applied to many different gear systems, including time-variant ones. In order to verify the model proposed in Section 5-(2), a simulation is performed in the conditions imposed by the most restrictive model, namely the open differential from Matlab/Simulink: $J_e = 0$, $J_c = 0$ in matrix $\mathbf{J}$ in (4) and $b_e = 0$, $b_c = 0$ in matrix $\mathbf{B}_J$ in (4), together with no relative friction acting between any of the system gears and with the use of the

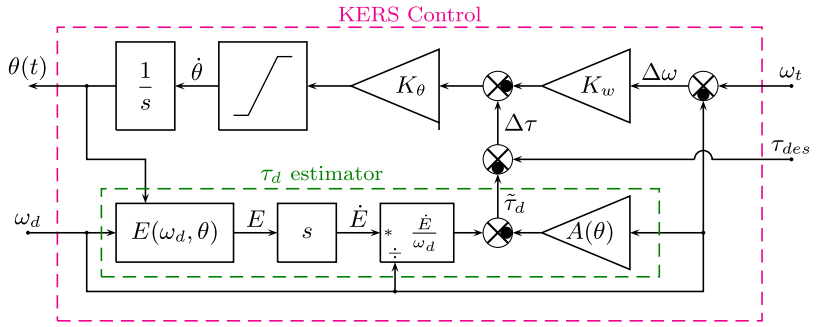

Fig. 9. Structure of the "KERS Control" algorithm.

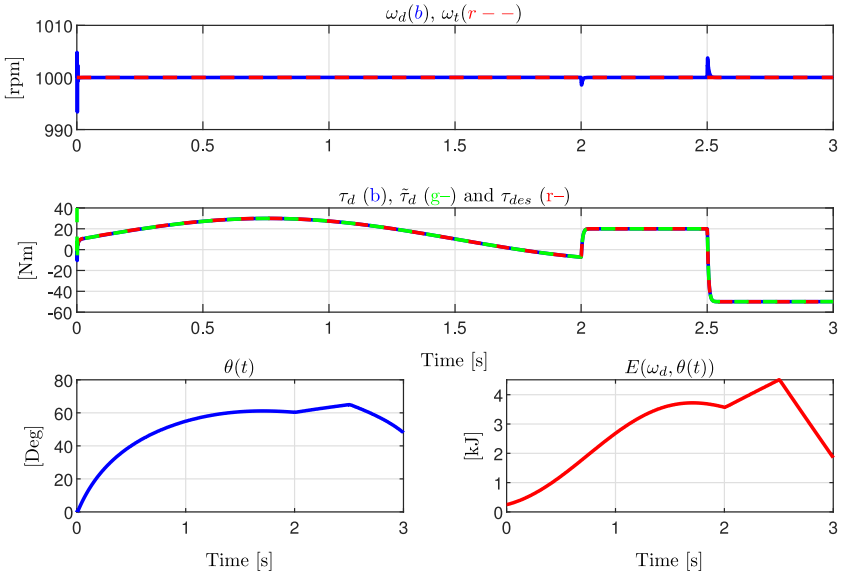

Fig. 10. Full toroidal variator: angular speeds, torques, control variable and stored energy.

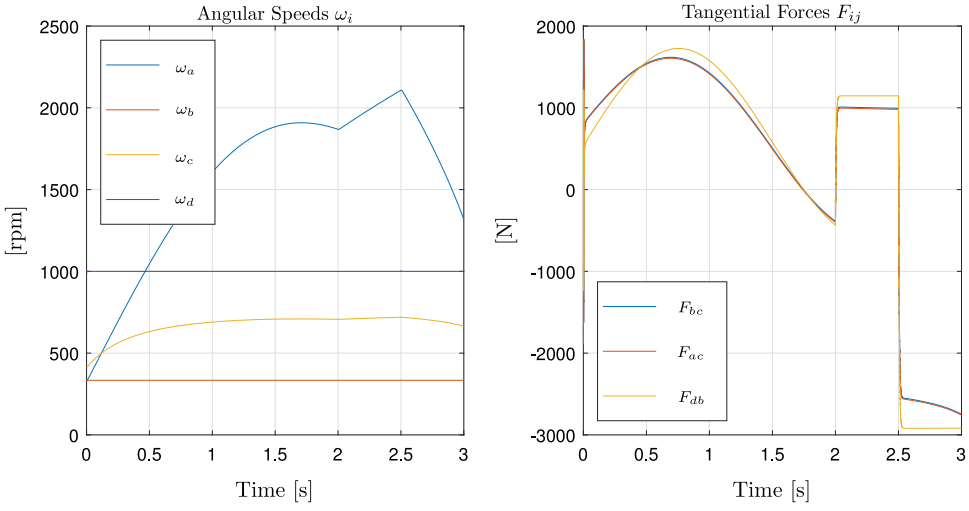

Fig. 11. Full toroidal variator: angular speeds and tangential forces.

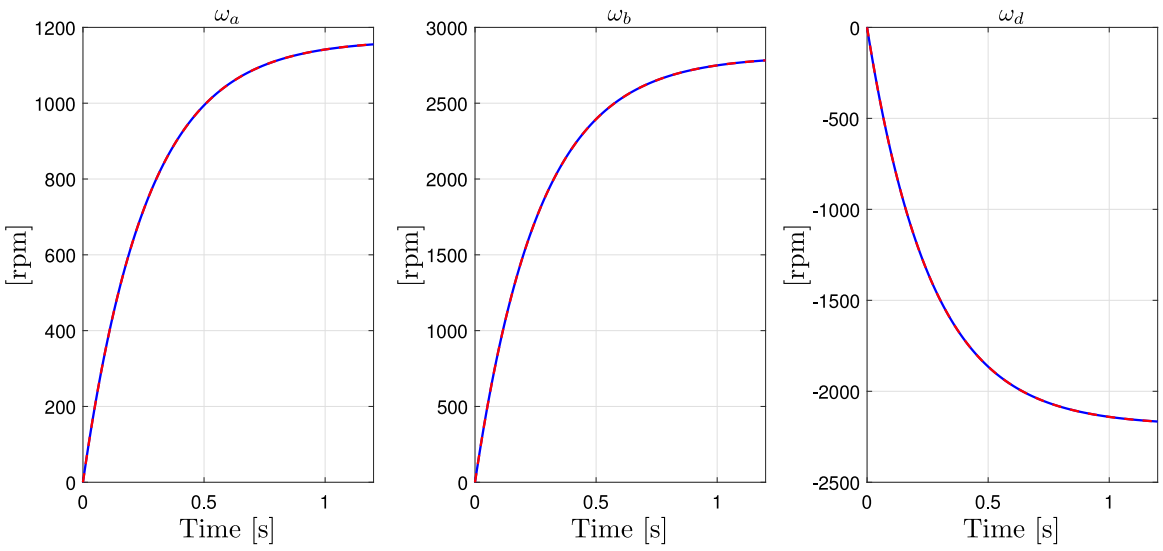

Fig. 12. Comparison of the simulation results: Matlab/Simulink (blue) and systematic POG-based model (red dashed).

reduced differential model (9) neglecting the gears elastic interaction. The simulation has been performed starting from zero initial conditions, applying an input torque $\tau_b = 100$ Nm and using the values reported in Table 1. The results are reported in Fig. 12 in terms of angular speeds ω_a, ω_b and ω_d.

From the simulations and from observations (a), (b), (c) and (d) reported above, two conclusions can be evinced: the systematic POG-based model is correct and more complete than the Matlab/Simulink open differential model.

(2) Full Toroidal Variator. The full toroidal variator shown in Fig. 7 can also be modeled using other approaches. One of the most common approaches in the literature for modeling mechanical systems is the Lagrangian approach (Pesce, 2003; Pesce, Tannuri, & Casetta, 2006), but this can only be applied to rigid systems composed of constant masses or constant moments of inertia. The reduced model of the considered full toroidal variator behaves as a system with time-variant moment of inertia $J(t)$, as shown in (22). In order to model time-variant dynamic systems, it is necessary to use the so-called extended Lagrangian equations (Pesce, 2003; Pesce et al., 2006):

$$\frac{d}{dt}\left(\frac{\partial T}{\partial \dot{q}_i}\right) - \frac{\partial T}{\partial q_i} + \frac{\partial U}{\partial q_i} = Q_i - \frac{1}{2}\dot{J}(t)\dot{q}_i, \quad i = 1, \dots, N, \tag{24}$$

where N is the number of the system degrees of freedom, q_i are the generalized Lagrangian coordinates, Q_i are the generalized forces, T and U are the system kinetic and potential energies. For the considered system, one obtains:

$$\begin{aligned} &T = \tfrac{1}{2}J(t)\omega_d^2, \quad U = 0, \quad Q_1 = (\tau_d - b_d R_d \omega_d)R_d + \\ &+(\tau_c - b_c R_{c\theta}\omega_d)R_{c\theta} + (\tau_b - b_b R_b \omega_d)R_b + (\tau_a - b_a R_{a\theta}\omega_d)R_{a\theta}, \end{aligned} \tag{25}$$

$q_1 = \theta_d$, namely the angular position of the time-variant inertia $J(t)$ in (22). Note that having a moment of inertia $J(t)$ dependent on time through a function $\theta(t)$ implies that an additional term needs to be added to the generalized force Q_1, as shown in (24). By applying (24), and using T, U and Q_1 defined in (25), the reader can verify that the same time-variant differential equation as in (22) is obtained. The systematic modeling approach proposed in this paper offers the following benefits compared to the generalized Lagrangian approach: (a) the systematic rules to follow are always the same both for systems with constant inertia and for systems with time-variant inertia. This means that the modeling process can be automatized applying the rules and algorithms presented in this paper without worrying about distinguishing different cases; (b) the Lagrangian approach requires the exact manual computation of the kinetic energy T and of the generalized forces terms Q_i in (24), including coefficients $R_{a\theta}$, R_b, $R_{c\theta}$, R_d, which may become quite complex expressions especially if the number and the types of frictions (e.g. relative frictions) affecting the system increase. Using the systematic approach proposed in this paper, coefficients $R_{a\theta}$, R_b, $R_{c\theta}$, R_d are determined automatically, see (21). Furthermore, it can also become quite complex to determine the correct sign of the different terms within the generalized forces Q_i, which is important in order to distinguish motive torques from friction torques. On the contrary, the proposed approach allows to systematically obtain the terms $\mathbf{A}_1(t)$ and $\mathbf{B}_1(t)$ in (9) (which compose the generalized forces Q_i in (24)), and is therefore less prone to calculation mistakes. Additionally, note that the computation of the dissipated power and of the stored energy is straightforward with the proposed approach, see (3); (c) the proposed approach allows to automatically and systematically obtain two models of the system at the same time: a full one, giving a more detailed description of the system including the gears elastic interaction, and a reduced order one assuming rigid connections. The reduced model automatically gives the kinematic relations between the gears angular speeds and input torques. Furthermore, it is more suitable for fixed-step size simulations for real-time executions, as it does not contain the stiffnesses faster dynamics; (d) the time behavior of the forces exchanged between the gears can still be computed in the reduced model using (11).

8. Conclusion

In this paper, a systematic methodology for modeling complex time-variant gear systems has been proposed. This approach enables the systematic and automatic modeling of a large variety of gear systems, including planetary gear sets, bevel gearing system having perpendicular or non-perpendicular rotation axes (used to model vehicle differentials and many other systems), as well as time-variant systems, such as half or full toroidal variators, etc. The proposed methodology gives two system models with different degrees of detail: a full model including the gears elastic interaction and a reduced rigid model. Both models can be derived using a fully systematic procedure and can be directly implemented in the Matlab/Simulink environment employing the same unified structure. The reduced model is suitable for fixed-step simulations in real-time execution, since no fast dynamics due to the tangential springs is present. Furthermore, the kinematic equations of the considered gear system are automatically highlighted in the reduced model, and the time behavior of the tangential forces can still be computed. The system matrices and vectors can be automatically computed; in particular, two algorithms have been proposed for the

automatic computation of matrices $\mathbf{R}(t)$ and $\mathbf{B}_{\Delta\omega}$. The user can freely decide whether to account for relative frictions between couples of system gears. In order to show the wide range of gear systems which this methodology can be applied to, the modeling of three different gear systems has been addressed in this paper: a fictitious differential structure including a bevel gearing system with non-perpendicular gear shafts, a vehicle differential and a time-variant system such as a full toroidal variator. The simulations of these systems highlight the good matching between the results given by the full and reduced system models. As far as the full toroidal variator is concerned, its control when employed as a KERS has also been addressed with reference to an automotive case study. Finally, the comparison of the proposed modeling methodology with two other approaches has been addressed.

Declaration of competing interest

The authors declare that they have no known competing financial interests or personal relationships that could have appeared to influence the work reported in this paper.

Funding

This research did not receive any specific grant from funding agencies in the public, commercial, or not-for-profit sectors.

Appendix A. Algorithm 2 for the calculation of matrix $\mathbf{B}_{\Delta\omega}$

The generic coefficient B_{ij} of matrix $\mathbf{B}_{\Delta\omega}=[B_{ij}]$, with $i,j\in\mathcal{N}_J$ and set $\mathcal{N}_J$ defined in (1), can be computed as:

$$B_{ij}=\begin{cases}\displaystyle\sum_{pq\in\mathcal{N}_i} b_{pq} & \text{if} \quad i=j,\\ S_{ij}\bar{b}_{ij} & \text{if} \quad i\neq j,\end{cases} \tag{A.1}$$

where $\mathcal{N}_i$ is a set of subscripts "pq" defined as follows:

$\mathcal{N}_i=\{$all the subscripts $pq\in\mathcal{N}_B$ such that $p=i$ or $q=i\}$

$\mathcal{N}_B$ is defined in (1), $\bar{b}_{ij}$ and S_{ij} are the relative friction coefficient and a sign function defined as, respectively:

$$\bar{b}_{ij}=\begin{cases}b_{ij} & \text{if } ij\in\mathcal{N}_B,\\ b_{ji} & \text{if } ji\in\mathcal{N}_B,\\ 0 & \text{if otherwise,}\end{cases} \qquad S_{ij}=\begin{cases}-1 & \text{if } \omega_i,\ \omega_j \text{ have the same positive direction,}\\ 1 & \text{if } \omega_i,\ \omega_j \text{ have different positive direction,}\\ 0 & \text{if } \bar{b}_{ij}=0.\end{cases}$$

Appendix B. Proof of Property 2

The notation "(t)" showing the time dependence of the time-variant terms will be omitted in this proof for the sake of brevity. The first equation of (2) can be rewritten as follows:

$$\mathbf{R}^{\mathrm{T}}\mathbf{F}=\boldsymbol{\tau}-\mathbf{J}\dot{\boldsymbol{\omega}}-(\mathbf{B}_J+\mathbf{R}^{\mathrm{T}}\mathbf{B}_K\mathbf{R})\boldsymbol{\omega}. \tag{B.1}$$

When $\mathbf{K}\to\infty$, from (7) and (8) it follows: $\boldsymbol{\omega}=\mathbf{Q}_1\mathbf{x}_1$, which implies $\dot{\boldsymbol{\omega}}=\dot{\mathbf{Q}}_1\mathbf{x}_1+\mathbf{Q}_1\dot{\mathbf{x}}_1$. By replacing $\boldsymbol{\omega}$ and $\dot{\boldsymbol{\omega}}$ in (B.1), it is:

$$\mathbf{R}^{\mathrm{T}}\mathbf{F}=\boldsymbol{\tau}-\mathbf{J}\mathbf{Q}_1\dot{\mathbf{x}}_1-\mathbf{B}_J\mathbf{Q}_1\mathbf{x}_1-\mathbf{R}^{\mathrm{T}}\mathbf{B}_K\underbrace{\mathbf{R}\mathbf{Q}_1}_{\mathbf{0}}\mathbf{x}_1-\mathbf{J}\dot{\mathbf{Q}}_1\mathbf{x}_1. \tag{B.2}$$

By substituting the time derivative $\dot{\mathbf{x}}_1=\mathbf{L}_1^{-1}\mathbf{A}_1\mathbf{x}_1+\mathbf{L}_1^{-1}\mathbf{B}_1\boldsymbol{\tau}-\mathbf{L}_1^{-1}\mathbf{N}_1\mathbf{x}_1$ obtained from (9) in (B.2), one obtains:

$$\begin{aligned}\mathbf{R}^{\mathrm{T}}\mathbf{F}=&(\mathbf{I}-\mathbf{J}\mathbf{Q}_1\mathbf{L}_1^{-1}\mathbf{B}_1)\boldsymbol{\tau}+\\ &-(\mathbf{B}_J\mathbf{Q}_1+\mathbf{J}\mathbf{Q}_1\mathbf{L}_1^{-1}\mathbf{A}_1-\mathbf{J}\mathbf{Q}_1\mathbf{L}_1^{-1}\mathbf{N}_1+\mathbf{J}\dot{\mathbf{Q}}_1)\mathbf{x}_1.\end{aligned} \tag{B.3}$$

By substituting matrices $\mathbf{L}_1$, $\mathbf{N}_1$, $\mathbf{A}_1$ and $\mathbf{B}_1$ given in (10) within (B.3) and doing some algebra, one obtains:

$$\mathbf{R}^{\mathrm{T}}\mathbf{F}=\underbrace{(\mathbf{I}-\mathbf{J}\mathbf{Q}_1(\mathbf{Q}_1^{\mathrm{T}}\mathbf{J}\mathbf{Q}_1)^{-1}\mathbf{Q}_1^{\mathrm{T}})}_{\mathbf{M}_p}(\boldsymbol{\tau}-\mathbf{B}_J\mathbf{Q}_1\mathbf{x}_1-\mathbf{J}\dot{\mathbf{Q}}_1\mathbf{x}_1). \tag{B.4}$$

Matrix $\mathbf{M}_p$ in (B.4) is a projection matrix on $\ker(\mathbf{Q}_1^T)$ along $\mathrm{Im}(\mathbf{J}\mathbf{Q}_1)$. Matrix $\mathbf{M}_p$ can also be rewritten as follows:

$$\mathbf{M}_p=\mathbf{P}(\mathbf{S}^{\mathrm{T}}\mathbf{P})^{-1}\mathbf{S}^{\mathrm{T}}, \tag{B.5}$$

where matrices $\mathbf{P}$ and $\mathbf{S}$ can be determined by solving:

$$\ker(\mathbf{Q}_1^T)=\mathrm{Im}(\mathbf{P}). \tag{B.6}$$

$$\mathrm{Im}(\mathbf{J}\mathbf{Q}_1)=\ker(\mathbf{S}^{\mathrm{T}}). \tag{B.7}$$

Eq. (B.6) can be solved as in the following. From (7), it follows:

$$\mathbf{R}\boldsymbol{\omega}=\mathbf{0}\leftrightarrow\mathbf{R}\mathbf{Q}_1\mathbf{x}_1=\mathbf{0}\leftrightarrow\mathbf{R}\mathbf{Q}_1=\mathbf{0}\leftrightarrow\mathbf{Q}_1^{\mathrm{T}}\mathbf{R}^{\mathrm{T}}=\mathbf{0},$$

which implies $\ker(\mathbf{Q}_1^{\mathrm{T}})=\mathrm{Im}(\mathbf{R}^{\mathrm{T}})$. Replacing $\ker(\mathbf{Q}_1^{\mathrm{T}})=\mathrm{Im}(\mathbf{R}^{\mathrm{T}})$ in (B.6) results in $\mathbf{P}=\mathbf{R}^{\mathrm{T}}$.

Eq. (B.7) can be solved as in the following. From the equality $\mathbf{Q}_1^{\mathrm{T}}\mathbf{R}^{\mathrm{T}}=\mathbf{0}$ introduced in the solution of Eq. (B.6), it follows:

$$\mathbf{Q}_1^{\mathrm{T}}\mathbf{J}\mathbf{J}^{-1}\mathbf{R}^{\mathrm{T}}=\mathbf{0}\leftrightarrow\left(\mathbf{J}^{-1}\mathbf{R}^{\mathrm{T}}\right)^{\mathrm{T}}(\mathbf{Q}_1^{\mathrm{T}}\mathbf{J})^{\mathrm{T}}=\mathbf{0}\leftrightarrow\left(\mathbf{J}^{-1}\mathbf{R}^{\mathrm{T}}\right)^{\mathrm{T}}(\mathbf{J}\mathbf{Q}_1)=\mathbf{0},$$

which implies $\ker\left[\left(\mathbf{J}^{-1}\mathbf{R}^{\mathrm{T}}\right)^{\mathrm{T}}\right]=\mathrm{Im}(\mathbf{J}\mathbf{Q}_1)$. Replacing $\ker\left[\left(\mathbf{J}^{-1}\mathbf{R}^{\mathrm{T}}\right)^{\mathrm{T}}\right]=\mathrm{Im}(\mathbf{J}\mathbf{Q}_1)$ in (B.7) results in $\mathbf{S}=\mathbf{J}^{-1}\mathbf{R}^{\mathrm{T}}$.

Replacing $\mathbf{P}=\mathbf{R}^{\mathrm{T}}$ and $\mathbf{S}=\mathbf{J}^{-1}\mathbf{R}^{\mathrm{T}}$ in $\mathbf{M}_p$ in (B.5), it results $\mathbf{M}_p=\mathbf{R}^{\mathrm{T}}\left[(\mathbf{J}^{-1}\mathbf{R}^{\mathrm{T}})^{\mathrm{T}}\mathbf{R}^{\mathrm{T}}\right]^{-1}(\mathbf{J}^{-1}\mathbf{R}^{\mathrm{T}})^{\mathrm{T}}=\mathbf{R}^{\mathrm{T}}(\mathbf{R}\mathbf{J}^{-1}\mathbf{R}^{\mathrm{T}})^{-1}\mathbf{R}\mathbf{J}^{-1}$. Substituting the latter in (B.4), one obtains:

$$\mathbf{R}^{\mathrm{T}}\mathbf{F}=\underbrace{\mathbf{R}^{\mathrm{T}}(\mathbf{R}\mathbf{J}^{-1}\mathbf{R}^{\mathrm{T}})^{-1}\mathbf{R}\mathbf{J}^{-1}}_{\mathbf{M}_p}(\boldsymbol{\tau}-\mathbf{B}_J\mathbf{Q}_1\mathbf{x}_1-\mathbf{J}\dot{\mathbf{Q}}_1\mathbf{x}_1),$$

directly giving $\mathbf{F}=(\mathbf{R}\mathbf{J}^{-1}\mathbf{R}^{\mathrm{T}})^{-1}\mathbf{R}\mathbf{J}^{-1}\left[\boldsymbol{\tau}-\left(\mathbf{B}_J\mathbf{Q}_1+\mathbf{J}\dot{\mathbf{Q}}_1\right)\mathbf{x}_1\right]$ because $\mathbf{R}^{\mathrm{T}}$ is a full rank matrix, see Remark 2. □

Appendix C. Supplementary data

Supplementary material related to this article can be found online at https://doi.org/10.1016/j.conengprac.2022.105420.

References

Benford, H. L., & Leising, M. B. (1981). The level analogy: a new tool in transmission analysis. *SAE Transactions*, *90*(1), 429–437. http://dx.doi.org/10.4271/810102.

Cauffriez, L., Grondel, S., Loslever, P., & Aubrun, C. (2016). Bond Graph modeling for fault detection and isolation of a train door mechatronic system. *Control Engineering Practice*, *49*, 212–224. http://dx.doi.org/10.1016/j.conengprac.2015.12.019.

Chen, B., Evangelou, S. A., & Lot, R. (2019). Series hybrid electric vehicle simultaneous energy management and driving speed optimization. *IEEE/ASME Transactions on Mechatronics*, *24*(6), 2756–2767. http://dx.doi.org/10.1109/TMECH.2019.2943320.

Du, J., Mao, J., Cui, Y., Liu, K., & Zhao, G. (2018). Theoretical and experimental study on load sharing of a novel power split spiral bevel gear transmission. *Advances in Mechanical Engineering*, *10*(6), 1–9. http://dx.doi.org/10.1177/1687814018779490.

Forstinger, M., Bauer, R., Hofer, A., & Rossegger, W. (2016). Multivariable control of a test bed for differential gears. *Control Engineering Practice*, *57*, 18–28. http://dx.doi.org/10.1016/j.conengprac.2016.08.010.

Freudenstein, F., & Yang, A. T. (1972). Kinematics and statics of a coupled epicyclic spur-gear train. *Mechanism and Machine Throry*, *7*(2), 263–275. http://dx.doi.org/10.1016/0094-114X(72)90008-0.

Fuchs, R., Hasuda, Y., & James, I. (2002). *Full toroidal IVT variator dynamics*: *SAE Technical Paper 2002-(2002) 01-0586*, http://dx.doi.org/10.4271/2002-01-0586.

Gadola, M., & Chindamo, D. (2018). The mechanical limited-slip differential revisited: high-performance and racing car applications. *International Journal of Applied Engineering Research*, *13*(2), 1478–1495.

García-Herreros, I., Kestelyn, X., Gomand, J., Coleman, R., & Barre, P.-J. (2013). Model-based decoupling control method for dual-drive gantry stages: A case study with experimental validations. *Control Engineering Practice*, *21*(3), 298–307. http://dx.doi.org/10.1016/j.conengprac.2012.10.010.

Gong, X., Wang, J., Ma, B., Lu, L., Hu, Y., & Chen, H. (2021). Real-time integrated power and thermal management of connected HEVs based on hierarchical model predictive control. *IEEE/ASME Transactions on Mechatronics*, *26*(3), 1271–1282. http://dx.doi.org/10.1109/TMECH.2021.3070330.

He, H., Shou, Y., & Wang, H. (2022). Fuel economy optimization of diesel engine for plug-in hybrid electric vehicle based on equivalent operating points. *Control Engineering Practice*, *123*, http://dx.doi.org/10.1016/j.conengprac.2022.105162.

Hou, H., & Ji, H. (2021). Improved multiclass support vector data description for planetary gearbox fault diagnosis. *Control Engineering Practice*, *114*, http://dx.doi.org/10.1016/j.conengprac.2021.104867.

Jha, M.-S., Dauphin-Tanguy, G., & Ould-Bouamama, B. (2018). Robust fault detection with interval valued uncertainties in bond graph framework. *Control Engineering Practice*, *71*, 61–78. http://dx.doi.org/10.1016/j.conengprac.2017.10.009.

Khajepour, A., Fallah, M. S., & Goodarzi, A. (2014). *Electric and hybrid vehicles: technologies, modeling and control - a mechatronic approach*. John Wiley & Sons.

Kim, S., & Choi, S. B. (2020). Cooperative control of drive motor and clutch for gear shift of hybrid electric vehicles with dual-clutch transmission. *IEEE/ASME Transactions on Mechatronics*, *25*(3), 1578–1588. http://dx.doi.org/10.1109/TMECH.2020.2980120.

Lhomme, W., Bouscayrol, A., Syed, S. A., Roy, S., Gailly, F., & Pape, O. (2017). Energy savings of a hybrid truck using a ravigneaux gear train. *IEEE Transactions on Vehicular Technology*, *66*(10), 8682–8692. http://dx.doi.org/10.1109/TVT.2017.2710378.

Miller, J. M. (2006). Hybrid electric vehicle propulsion system architectures of the e-CVT type. *IEEE Transactions on Power Electronics*, *21*(3), 756–767. http://dx.doi.org/10.1109/TPEL.2006.872372.

Mishra, K. D., & Srinivasan, K. (2017). Robust control and estimation of clutch-to-clutch shifts. *Control Engineering Practice*, *65*, 100–114. http://dx.doi.org/10.1016/j.conengprac.2017.05.007.

Molyneux, W. G. (1997). The internal bevel gear and its applications. *Proceedings of the Institution of Mechanical Engineers, Part G: Journal of Aerospace Engineering*, *211*(1), 39–61. http://dx.doi.org/10.1243/0954410971532488.

Newall, J. P., Cowperthwaite, S., Hough, M., & Lee, A. P. (2005). Efficiency modelling in the full toroidal variator: investigation into optimisation of EHL contact conditions to maximize contact efficiency. *Tribology and Interface Engineering Series*, *48*, 245–255. http://dx.doi.org/10.1016/S0167-8922(05)80027-6.

Oncken, J., Sachdeva, K., Wang, H., & Chen, B. (2021). Integrated predictive powertrain control for a multi-mode plug-in hybrid electric vehicle. *IEEE/ASME Transactions on Mechatronics*, *26*(3), 1248–1259. http://dx.doi.org/10.1109/TMECH.2021.3061287.

Ouyang, T., Lu, Y., Li, S., Yang, R., Xu, P., & Chen, N. (2022). An improved smooth shift strategy for clutch mechanism of heavy tractor semi-trailer automatic transmission. *Control Engineering Practice*, *121*, http://dx.doi.org/10.1016/j.conengprac.2021.105040.

Patil, H. S. (2011). An experimental study on full toroidal continuously variable transmission system. *The International Journal of Advanced Manufacturing Technology*, *5*(1), 19–23.

Pesce, C. P. (2003). The application of lagrange equations to mechanical systems with mass explicitly dependent on position. *Journal of Applied Mechanics*, *70*(5), 751–756. http://dx.doi.org/10.1115/1.1601249.

Pesce, C. P., Tannuri, E. A., & Casetta, L. (2006). The Lagrange equations for systems with mass varying explicitly with position: some applications to offshore engineering. *Journal of the Brazilian Society of Mechanical Sciences and Engineering*, *28*(4), 496–504. http://dx.doi.org/10.1590/S1678-58782006000400015.

S., Documentation. 0000. Simulation and model-based design, MathWorks, https://it.mathworks.com/help/autoblks/ref/opendifferential.html.

S., Documentation. 0000. Simulation and model-based design, MathWorks, https://it.mathworks.com/help/autoblks/ref/limitedslipdifferential.html.

Tebaldi, D., & Zanasi, R. (2019). Modeling and control of a power-split hybrid propulsion system. In *IEEE 45th annual conference of the industrial electronics society* (pp. 14–17). Lisbon, Portugal: http://dx.doi.org/10.1109/IECON.2019.8927084.

Tebaldi, D., & Zanasi, R. (2021). Modeling control and simulation of a power- split hybrid wheel loader. In *Mediterranean conference on control and automation* (pp. 22–25). Puglia, Italy: http://dx.doi.org/10.1109/MED51440.2021.9480213.

Zanasi, R. (2010). The power-oriented graphs technique: system modeling and basic properties. In *IEEE vehicle power and propulsion conference, Lille, France* (pp. 1–3). http://dx.doi.org/10.1109/VPPC.2010.5729018.

Zanasi, R., Geitner, G. H., Bouscayrol, A., & Lhomme, W. (2008). Different energetic techniques for modelling traction drives. In *9th International conference on modeling and simulation of electric machines, converters and systems* (pp. 8–11). Québec, Canada.

Zanasi, R., Grossi, F., & Fei, M. (2014). Dynamic modeling of a full toroidal variator: the power-oriented graphs approach. In *IEEE European control conference* (pp. 24–27). Strasbourg, France: http://dx.doi.org/10.1109/ECC.2014.6862181.

Zanasi, R., & Tebaldi, D. (2019). Planetary gear modeling using the power-oriented graphs technique. In *IEEE European control conference* (pp. 25–28). Naples, Italy: http://dx.doi.org/10.23919/ECC.2019.8796006.

Zanasi, R., & Tebaldi, D. (2020a). Modeling of complex planetary gear sets using power-oriented graphs. *IEEE Transactions on Vehicular Technology*, *69*(12), 14470–14483. http://dx.doi.org/10.1109/TVT.2020.3040899.

Zanasi, R., & Tebaldi, D. (2020b). Power-oriented modeling of epicyclic gear trains. In *Vehicular power and propulsion conference* (pp. 26–29). Gijón, Spain: http://dx.doi.org/10.1109/VPPC49601.2020.9330971.

Zhang, X., Liu, H., Zhan, Z., Wu, Y., Zhang, W., Taha, M., et al. (2020). Modelling and active damping of engine torque ripple in a power-split hybrid electric vehicle. *Control Engineering Practice*, *104*, http://dx.doi.org/10.1016/j.conengprac.2020.104634.

Zhang, J., Shen, T., & Kako, J. (2020). Short-term optimal energy management of power-split hybrid electric vehicles under velocity tracking control. *IEEE Transactions on Vehicular Technology*, *69*(1), 182–193. http://dx.doi.org/10.1109/TVT.2019.2950042.